Theoretical Study of Excited States of DNA Base Dimers and Tetramers Using Optimally Tuned Range-Separated Density Functional Theory

Haitao Sun,*[a] Shian Zhang,[a] Cheng Zhong,[b] and Zhenrong Sun*[a]

Excited states of various DNA base dimers and tetramers including Watson-Crick H-bonding and stacking interactions have been investigated by time-dependent density functional theory using nonempirically tuned range-separated exchange (RSE) functionals. Significant improvements are found in the prediction of excitation energies and oscillator strengths, with results comparable to those of high-level coupled-cluster (CC) models (RI-CC2 and EOM-CCSD(T)). The optimally-tuned RSE functional significantly outperforms its non-tuned (default) version and widely-used B3LYP functional. Compared to those high-level CC benchmarks, the large mean absolute deviations of conventional functionals can be attributed to their inappropriate amount of exact exchange and large delocalization errors which can be greatly eliminated by tuning approach. Furthermore, the impacts of H-bonding and π-stacking interactions in various DNA dimers and tetramers are analyzed through peak shift of simulated absorption spectra as well as corresponding change of absorption intensity. The result indicates the stacking interaction in DNA tetramers mainly contributes to the hypochromicity effect. The present work provides an efficient theoretical tool for accurate prediction of optical properties and excited states of nucleobase and other biological systems. © 2015 Wiley Periodicals, Inc.

DOI: 10.1002/jcc.24266

Introduction

Fundamental understanding the excited electronic states and photophysical properties of DNA and RNA nucleic acid bases (NABs) has its significant biological importance and so far has attracted great attention.[1–6] For example, the formation of excited states of NABs by UV radiation is a primary step causing genetic damage; The charge transfer (CT) process[7] through a DNA strand plays a photoprotective role in enhancing its photostability,[8] which allows for DNA-based structures as promising materials for nanoelectronics.[9–11] However, due to the complex biological environment and flexible geometries of a DNA duplex, a comprehensive understanding of the crucial phenomena such as UV radiation-induced DNA damage and conductivity along DNA double helices remains a challenge.[12,13] First, it is of great importance to fully characterize the relationship between the optical properties and electronic structures of DNA molecules, as well as intra- and intermolecular interactions.[14] Although many experimental and theoretical efforts have focused on isolated DNA bases, systematic studies on base pairs and assemblies are relatively limited.[15] Kohler[16] pointed out that the photochemistry properties between isolated DNA bases and DNA chain are quite different and the relaxation in a DNA duplex is much slower than that in individual monomers. Miannay et al.[17] demonstrated that the behavior of excited-state relaxation in guanine-cytosine (GC) double helix contrasts with that in adenine-thymine (AT) duplex by comparing their fluorescence decays. Créspo-Hernandez et al. have shown the key role of stacking interaction in the control of the excited-state dynamics in an AT complex.[2] Therefore, DNA pairs and especially larger clusters, which combine hydrogen(H-) bonding and π-stacking interactions, are relevant prototypical systems to be studied since they can be seen as the basic building blocks of a realistic DNA duplex.[18] From a theoretical perspective care must be taken, however, in choosing an appropriate level of theory that is capable of providing both efficient and accurate prediction of the excited-state properties of the DNA building blocks.[19]

Various computational approaches from low to high levels of theory have been performed to describe the excitation spectrum and excited-state relaxation of NABs.[20–23] These methods may be divided into two categories: "inexpensive but rough" and "accurate but expensive." The former type, such as configuration interaction singles (CIS) and latter-developed intermediate neglect of differential overlap-spectroscopic parameterization (INDO/S) semi-empirical quantum chemistry

[a] H. Sun, S. Zhang, Z. Sun
State Key Laboratory of Precision Spectroscopy, Department of Physics, East China Normal University, Shanghai 200062, People's Republic of China
E-mail: htsun@phy.ecnu.edu.cn or zrsun@phy.ecnu.edu.cn
[b] C. Zhong
Department of Chemistry, Wuhan University, Hubei 430072, People's Republic of China

Contract grant sponsor: China Postdoctoral Science Foundation; Contract grant number: 2014M561435; Contract grant sponsor: National Natural Science Fund; Contract grant numbers: 11004060, , 11474096 and 1027403; Contract grant sponsor: Shanghai Municipal Science and Technology Commission; Contract grant number: 14JC1401500; Contract grant sponsor: Shanghai Rising-Star Program; Contract grant number: 12QA1400900

methods,[23] can be applied to large biological system but is mostly restricted to a qualitative study. The latter type such as post-Hartree-Fock (PHF) methods can allow for accurate prediction of excited-state properties due to their inclusion of sufficient electron correlation and is commonly employed as high-level benchmarking methods.[24] However, the careful choice of active space in the multi-configurational second-order perturbation approach (CASPT2) and particularly the very high computational cost using coupled-cluster (CC) methods limit their applicability as a routine calculation. More importantly, there is a great need to develop reliable approximate methods that can be applied for long DNA strands beyond isolated bases, since the high-level PHF methods are typically too expensive to be feasible. Fortunately, time-dependent density functional theory (TDDFT)[25,26] has become a popular tool for calculations of excitation spectra and molecular response properties, due to the attractive scaling of computational requirements.[27] A common view has been emphasized that choosing a reliable approximation for the exchange-correlation (XC) potential is essential to determine the success or failure of TDDFT.[28] For example, TDDFT calculations with standard approximations (e.g., global hybrid B3LYP functional) have been shown to provide accurate prediction of the valence excitations of molecules.[25,29] However, while calculating charge-transfer molecules, those conventional functionals do not achieve sufficient accuracy in describing the CT excitation energies. This is also known as the classic breakdown of TDDFT.[30] It has been further demonstrated that even π–π^* valence transitions in some polycyclic aromatic hydrocarbon molecules also suffer a "CT-like" issue.[28,31] Generally, one can attribute the severe systematic errors in the calculated results to the introduction of inappropriate approximations in TDDFT. Furthermore, they can be traced back to large delocalization error (DE)[32] and lack of derivative discontinuity (DD),[33] and an incorrect asymptotic behavior of the potential.[34,35]

Recently, density functionals with range-separated exchange (RSE)[35,36] switching from DFT to HF at increasing interelectronic distances have been developed with intent of alleviating the CT problem of TDDFT.[37] For example, Lange et al.[38] pointed out the necessity of using RSE functionals for proper description of CT states of adenine dimer. Jensen and Govind[12] showed that RSE functionals significantly outperform conventional functionals for the calculations of excitation energies of DNA base pairs due to the full (100%) exact exchange (eX) in the long-range limit. Significant improvements are also found in prediction of excited states of other organic π-conjugated systems using the RSE approach.[12,39,40] In these functionals, the interelectronic repulsion is separated into short- and long-range domain, which is given for the interelectronic distance r_{12} as:[34]

$$\frac{1}{r_{12}} = \frac{1-[\alpha+\beta\mathrm{erf}\,(\omega r_{12})]}{r_{12}} + \frac{\alpha+\beta\mathrm{erf}\,(\omega r_{12})}{r_{12}} \quad (1)$$

The exchange is split into long-range eX component and short-range DFT component of the exchange. The parameter α in eq. (1) quantifies the fraction of eX in the short-range limit, while $\alpha+\beta$ gives the fraction of eX in the long-range limit. The range-separation parameter ω is the inverse of a distance at which the functional switches from DFT-like to HF-like. Typically for a RSE functional such as LC-ωPBE and ωB97X, $\alpha+\beta$ equals 1, indicating 100% eX in the long-range limit and guaranteeing an asymptotically correct behavior of functional. Furthermore, the parameter ω in RSE functionals can be considered as a function of the density[41,42] and has been shown to be strongly system-dependent.[43,44] Baer, Kronik, and coworkers have considered a nonempirical criterion to determine the optimal ω based on RSE functionals.[45] This concept of "optimal tuning" is to adjust ω to fulfill a fundamental DFT requirement: in exact Kohn-Sham (KS) or generalized KS (GKS) theory, for an N-electron system the negative of highest occupied molecular orbital (HOMO) energy, $-\varepsilon_H(N)$, is equal to the ionization potential (IP) exactly.[46] An optimal ω for RSE functionals is nonempirically determined to satisfy the above condition by minimizing $|\varepsilon_H(N)+\mathrm{IP}|$. For donor-acceptor systems, an improved eq. (2) was used as shown below:

$$J^2 = \sum_{i=0}^{1} [\varepsilon_H(N+i) + \mathrm{IP}(N+i)]^2 \quad (2)$$

This expression not only considers the IP of N-electron neutral system but also the IP of $N+1$ anion system. By considering the IP of $N+1$ anion, we can circumvent the issue of nonexistence of an analogous theorem that relates the lowest unoccupied molecular orbital (LUMO) of neutral system to its corresponding electron affinity (EA). The IP of $N+1$ anion can be then approximately considered as the EA of neutral system if ignoring relaxation effects. Therefore, the more refined eq. (2) can benefit properties that depend on not only HOMO energy but also on LUMO energy of N-electron system. Our earlier work has demonstrated that vertical ionization potentials of various adenine-thymine pairs and clusters can be well described using this "tuning" method.[18] Moore et al.[47] have demonstrated that the optimal tuning approach allows to obtain accurate excitation energies without degrading the description of band shapes for a set of small organic molecules. In addition, the tuned RSE method has been successfully used in other cases considered challenging for TDDFT, such as Rydberg and CT excitations.[13,28,44] Wong and coworkers calculated excitation energies of individual DNA monomers and dimers using this tuned RSE approach and achieved good accuracy compared to the high-level benchmark results.[13,48] However, they also mentioned that accuracy seems to be closely related to the amount of short- and long-range eX included in the functional.[48] In other words, the range separation parameter ω as well as the parameters α and β ($=1-\alpha$) are necessary to be adjusted to obtain "better" accuracy. If considering only ω tuning as "one-dimensional" (1D) tuning, adjusting the parameters ω and α simultaneously to minimize J^2 (as close to zero) in eq. (2) can be seen as "two-dimensional" (2D) tuning.[49]

In this work, we performed TDDFT calculations to obtain different types of excitation energies, including n–π^*excitation,

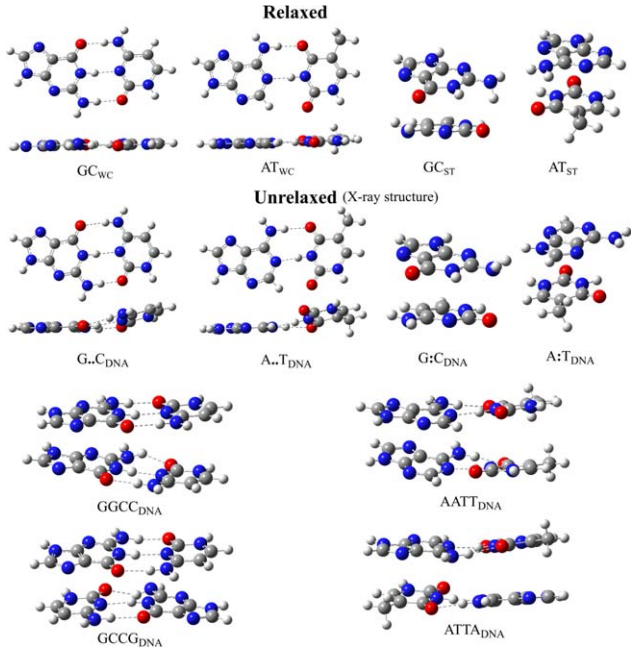

Figure 1. Molecular structures of various isomers of DNA dimers and tetramers (G: Guanine; C: Cytosine; T: Thymine; A: Adenine; WC(.): Watson-Crick; ST(:): stacked; DNA: X-ray structure of DNA duplex).

π–π^* localized excitation ($LE_{\pi\pi^*}$) and π–π^* CT excitation ($CT_{\pi\pi^*}$) of Watson-Crick (WC) base pairs and stacked complexes (molecular structures shown in Fig. 1). First, we show that the optimally-tuned RSE functionals have the overall improved predictive power not only for the well-publicized CT issue but also for n–π^* and $LE_{\pi\pi^*}$ transitions, significantly outperforming conventional density functionals. The reliability of the tuning approach can then be explored in larger tetramers whose structures are directly extracted from X-ray DNA duplex. By the assistance of tuning method, we then analyze the impact of H-bonding and π-stacking interactions by simulating the absorption spectra of various DNA base dimers and tetramers. Finally, we summarize the results of the present work and provide useful insights for the design of DNA-based materials for future applications in biology and bioelectronics.

Computational Details

The ground-state geometries of DNA dimers (GC_{WC}, GC_{ST}, AT_{WC}, and AT_{ST} as shown in Fig. 1) are optimized at the "resolution-of-identity" second-order Møller-Plesset perturbation (RI-MP2) level, taken from the work of Šponer et al.[50] To simulate a more realistic DNA model, the unrelaxed geometries of dimers and tetramers ($G.C_{DNA}$, $G:C_{DNA}$, $A.T_{DNA}$, $A:T_{DNA}$, $GGCC_{DNA}$, $GCCG_{DNA}$, $AATT_{DNA}$, and $ATTA_{DNA}$) are originally extracted from X-ray structure of the water-solvated DNA duplex (see Supporting Information Fig. S1).[51] Since hydrogen atoms are not resolved in the X-ray structures, they were added manually and their positions were optimized at the ωB97X-D/6-31+G(d,p) level.[52] All the geometries are documented in the Supporting Information.

The excitation energies of 30 singlet excited states were calculated at the TDDFT/cc-pVTZ level. The polarized triple-ζ cc-pVTZ basis set has been successfully applied in the computations of ground- and excited-state properties of DNA-based systems due to the accuracy of results accompanying with reasonable computational cost.[12,13,52,53] A Gaussian broadening (0.667 eV full width at half maximum) was applied to simulate the corresponding electronic absorption spectra. Computations of excitation energies with coupled cluster singles and doubles model using the resolution-of-identity approximation (RI-CC2) were carried out using the Turbomole code,[54] with TZVP basis set and SV(P) auxiliary basis set. Benchmark values using equation of motion coupled-cluster method with single and double as well as approximate triple excitations EOM-CCSD(T) were taken from the work of Szalay et al.[19] The behavior of delocalization error was investigated by calculating energies of DNA pairs as a function of fractional electron numbers using the NWChem package.[55]

Part of this work is mainly concerned with the parameter-optimization of RSE functionals. Optimal ω values listed in Table 1 were determined for all the DNA systems with two types of RSE functionals: LC-ωPBE[56] ($\alpha = 0.00$, $\beta = 1.00$, $\omega = 0.400$) and ωB97X[57] ($\alpha = 0.16$, $\beta = 0.84$, $\omega = 0.300$). As indicated in the Introduction, LC-ωPBE and ωB97X functionals contain 0% $\sim$ 100% and 16% $\sim$ 100% eX, respectively, from short to long-range limit. Hereafter we refer the optimally tuned RSE functionals with a symbol of asterisk (LC-ωPBE* and ωB97X*) to distinguish the default versions. All the single-point calculations were carried out for the neutral (N), cation and anion ($N \pm 1$) systems using default SCF convergence criteria in Gaussian 09 software.[58] The minimization of J^2 in eq. (2) is conventionally carried out by so-called fitting method which requires a large number of single-point calculations of neutral, cation, and anion systems (as illustrated in Supporting Information Fig. S2). In other words, this will somewhat limit the efficiency of tuning method. In this work, we have implemented the "golden ratio" method based on the Brent's algorithm (see Supporting Information for details) and use it to minimize the J^2 values with fewer steps and finer accuracy of ω values. All the tuning calculations were performed and analyzed using "xtune_g09" script provided as a supporting material in this work.

Table 1. Optimal ω values (Bohr^{-1}) tuned for various isomers of DNA pairs and quartets with the cc-pVTZ basis set, values in parentheses are for structures extracted from X-ray DNA helix.

System	Optimal ω ωB97X	Optimal ω LC-ωPBE
Default	0.300	0.400
GC_{WC}	0.218 (0.218)	0.251
GC_{ST}	0.214 (0.216)	0.248
AT_{WC}	0.218 (0.218)	0.252
AT_{ST}	0.213 (0.217)	0.243
$AATT_{DNA}$	0.185	–
$ATTA_{DNA}$	0.193	–
$GGCC_{DNA}$	0.180	–
$GCCG_{DNA}$	0.198	–

Table 2. Vertical excitation energies E_{ex} (eV) and oscillator strengths f (au) for six lowest singlet excited states of various GC and AT pairs using different methods.[a]

		B3LYP		LC-ωPBE		LC-ωPBE*		ωB97X*		RI-CC2		EOM-CCSD(T)	
States	Type	E_{ex}	f	E_{ex}	f	E_{ex}	f	E_{ex}	f	E_{ex}	f	E_{ex}	f
GC_{WC}													
G $\pi\rightarrow\pi^*$	LE	4.86	0.10	5.27	0.08	4.95	0.08	5.05	0.08	4.99	0.06	4.85	0.07
C $\pi\rightarrow\pi^*$	LE	4.90	0.04	5.39	0.14	5.06	0.08	5.19	0.09	5.04	0.06	4.92	0.10
G$\pi\rightarrow$Cπ^*	CT	3.38	0.00	6.49	0.00	5.38	0.01	5.45	0.01	5.33	0.03	5.36	0.01
G $\pi\rightarrow\pi^*$	LE	5.24	0.29	5.83	0.49	5.46	0.39	5.55	0.41	5.57	0.40	5.48	0.41
C $n\rightarrow\pi^*$	$n\pi^*$	4.79	0.00	5.93	0.00	5.36	0.00	5.59	0.00	5.54	0.00	5.65	0.00
G $n\rightarrow\pi^*$	$n\pi^*$	5.58	0.00	5.99	0.00	5.62	0.00	5.82	0.00	5.77	0.00	5.76	0.00
GC_{ST}													
C $\pi\rightarrow\pi^*$	LE	4.73	0.02	5.22	0.04	4.86	0.02	4.97	0.02	4.84	0.03	4.83	0.05
G $\pi\rightarrow\pi^*$	LE	4.95	0.07	5.33	0.08	4.99	0.04	5.04	0.03	5.14	0.05	5.04	0.04
C $n\rightarrow\pi^*$	$n\pi^*$	4.88	0.01	5.43	0.02	4.89[b]	0.00	5.17	0.03	5.06	0.01	5.20	0.03
G$\pi\rightarrow\pi^*$C	CT	4.04	0.00	5.96	0.06	5.14[c]	0.06	5.23	0.07	5.36	0.12	5.42	0.15
G $n\rightarrow\pi^*$	$n\pi^*$	5.24	0.00	5.60	0.00	5.28	0.00	5.47	0.00	5.42	0.01	5.51	0.00
G $\pi\rightarrow\pi^*$	LE	5.06	0.15	5.78	0.27	5.36	0.20	5.45	0.21	5.54	0.19	5.57	0.21
AT_{WC}													
T $n\rightarrow\pi^*$	$n\pi^*$	4.84	0.00	5.44	0.00	5.03	0.00	5.22	0.00	5.09	0.00	–	–
T $\pi\rightarrow\pi^*$	LE	4.98	0.08	5.38	0.20	5.05	0.15	5.17	0.18	5.28	0.16	–	–
A $\pi\rightarrow\pi^*$	LE	5.24	0.07	5.54	0.08	5.28	0.12	5.38	0.07	5.26	0.11	–	–
A $\pi\rightarrow\pi^*$	LE	4.94[d]	0.24	5.57	0.28	5.22	0.19	5.30	0.24	5.38	0.24	–	–
A $n\rightarrow\pi^*$	$n\pi^*$	5.15	0.00	5.75	0.00	5.21	0.00	5.46	0.00	5.49	0.00	–	–
A$\pi\rightarrow\pi^*$T	CT	4.24	0.00	7.28	0.01	6.03	0.01	6.12	0.00	6.10	0.02	–	–
AT_{ST}													
T $n\rightarrow\pi^*$	$n\pi^*$	4.79	0.00	5.26	0.00	4.86	0.00	5.06	0.00	4.98	0.00	5.04	0.00
A $\pi\rightarrow\pi^*$	LE	5.24	0.04	5.59	0.07	5.25	0.04	5.38	0.03	5.15	0.01	5.13	0.00
T/A$\pi\rightarrow\pi^*$	LE	4.90	0.01	5.35[e]	0.03	5.02[e]	0.02	5.12[e]	0.02	5.24	0.03	5.23	0.02
A $n\rightarrow\pi^*$	$n\pi^*$	4.88	0.01	5.46	0.01	4.88	0.00	5.18	0.01	5.28	0.00	5.31	0.00
T/A$\pi\rightarrow\pi^*$	LE	5.04	0.17	5.54	0.25	5.17	0.17	5.28	0.21	5.41	0.30	5.46	0.34
A$\pi\rightarrow\pi^*$T	CT	4.34	0.03	6.31	0.04	5.30[f]	0.08	5.41[f]	0.07	5.73	0.05	5.88	0.05
MAD	$n\pi^*$	0.31	−	0.28	+	0.19	−	0.08	+	0.06[g]	−		
MAD LE ($\pi\pi^*$)		0.25	−	0.25	+	0.12	−	0.12	+	0.05[g]	+		
W ($\pi\pi^*$)		0.09	−	0.32	+	0.06	+	0.15	+	0.06[g]	+		
B ($\pi\pi^*$)		0.41	−	0.21	+	0.17	−	0.08	−	0.05[g]	+		
MAD CT ($\pi\pi^*$)		1.63	−	0.88	+	0.19	−	0.15	−	0.08[g]	−		

[a] The sign + and − means that the calculated excitation energies are overestimated and underestimated, respectively, compared to the reference values. MAD values of DFT methods are compared to those of RI-CC2 methods. [b] Mixing G $\pi\rightarrow\pi^*$ C CT character. [c] Mixing G $\pi\rightarrow\pi^*$ character. [d] Mixing T $\pi\rightarrow\pi^*$ character. [e] Mixing A $\pi\rightarrow\pi^*$ T CT character. [f] Mixing A $\pi\rightarrow\pi^*$ character. [g] MAD values of RI-CC2 are compared to those of EOM-CCSD(T) taken from Szalay et al.[19]

Results and Discussion

This section is organized as follows: we first calculate the excitation energies and oscillator strengths of three types of transitions ($n\pi^*$, $LE_{\pi\pi^*}$, and $CT_{\pi\pi^*}$) for various optimized DNA dimers (GC_{ST}, GC_{WC}, AT_{ST}, and AT_{WC}) using TDDFT including the 1D optimally-tuned RSE functionals. The calculations of excitation energies based on 2D tuning were also performed in comparison to those of 1D tuning for GC_{ST} and GC_{WC}. Then we explore this tuning method for the calculations of excitation energies of four tetramers ($GGCC_{DNA}$, $GCCG_{DNA}$, $AATT_{DNA}$, and $ATTA_{DNA}$) whose structures are extracted from X-ray DNA duplex. The results are in comparison to those of B3LYP and RI-CC2 methods. We followingly analyze the performance of different functionals from the viewpoint of amount of eX and the corresponding DE of functional. After proving the reliability of tuning method in the description of excitation energies and oscillator strengths, the absorption spectra for both dimers and tetramers are thus simulated to analyze the effects of H-bonding and π-stacking interactions, as well as the hypochromicity effect.

The optimal range-separation parameters (ω) based on the two types of RSE functionals for AT and GC base pairs are listed in Table 1. Compared to the default ω values (0.400 $Bohr^{-1}$ for LC-ωPBE and 0.300 $Bohr^{-1}$ for ωB97X), the optimally tuned ω values significantly reduce to roughly 0.25 $Bohr^{-1}$ for LC-ωPBE and 0.21 $Bohr^{-1}$ for ωB97X, respectively. For larger tetramers, the ω values further decrease to 0.185 $\sim$ 0.198 $Bohr^{-1}$ for ωB97X. The results indicate that the tuning means is necessary for those DNA dimers and tetramers. A decreased ω value indicates that in the short region there is more composition of electron correlation than that of exact exchange, in other words, the short-range DFT is more slowly replaced by long-range exact exchange. The lowest excitation energies of four relaxed dimers calculated using different functionals are collected in Table 2. Results from an approximate coupled-cluster model RI-CC2 are also calculated in this work to assess the TDDFT excitation energies, since the reliable

experimental data for the absorption spectra is very limited. The benchmarking values by more accurate EOM-CCSD(T) method, taken from the work of Szalay et al.,[19] are used to assess the RI-CC2 and TDDFT results. The oscillator strength (f) is also calculated because (i) it provides another benchmark test for evaluation of excited-state properties and (ii) helps to determine the assignment of different types of transitions. First, we analyze the performance of different functionals on the calculations of three types of transitions including n–π^*, $LE_{\pi\pi^*}$ and $CT_{\pi\pi^*}$ excitations. The n–π^* transition is always accompanied with characteristic of very small (almost zero) oscillator strengths. The $LE_{\pi\pi^*}$ transition is recognized as a local excitation on one base while the CT transition distributes the HOMO on the one base and LUMO on the other one. As seen in Figure 2, compared to the excitation energies calculated by RI-CC2 method, the B3LYP functional underestimates all the three types of transitions with the mean absolute deviations (MADs) of 0.31 (n–π^*), 0.25 ($LE_{\pi\pi^*}$) and 1.63 ($CT_{\pi\pi^*}$) eV, respectively. In contrast, the non-tuned LC-ωPBE overestimates all the values with MADs of 0.27 (n–π^*), 0.25 ($LE_{\pi\pi^*}$), and 0.88 ($CT_{\pi\pi^*}$) eV, respectively. The deviations for n–π^* and $LE_{\pi\pi^*}$ transitions are still acceptable, however, both hybrid B3LYP and non-tuned LC-ωPBE functionals produce significantly large errors for the prediction of CT excitation energies. This finding is consistent with the previous studies in the literature.[12,13] Importantly, we find that the optimally-tuned LC-ωPBE* functional produces the results very comparable to those of the RI-CC2, and the MADs are 0.19 (n–π^*), 0.12 ($LE_{\pi\pi^*}$), and 0.19 ($CT_{\pi\pi^*}$) eV, respectively. The results using ωB97X* are slightly better, with MADs of 0.07 (n–π^*), 0.12 ($LE_{\pi\pi^*}$), and 0.15 ($CT_{\pi\pi^*}$) eV, respectively. In both cases, the MADs of n–π^* and $LE_{\pi\pi^*}$ transitions are reduced by more than half, and particularly the deviations of CT excitation energies are significantly reduced. Improvements are also found for the prediction of oscillator strengths by the tuning method. Interestingly, in the 6 lowest excited states of AT pairs and GC pairs, there are two localized π–π^* excitations located on adenine (A $\pi\rightarrow\pi^*$) and two located on guanine (G $\pi\rightarrow\pi^*$), labeled as bright "B" and weak "W," respectively, due to their relative oscillator strengths as shown in Table 2. As indicated in the Introduction, the hybrid B3LYP functional has been proved to produce accurate π–π^* valence excitation energies, which is also reflected in this work (by considering the moderate MAD of 0.24 eV using B3LYP). However, when local π–π^* transitions are separated into W and B types, the MAD of $LE_{\pi\pi^*}$ excitations of B type is 0.41 eV, significantly larger than the MAD of 0.09 eV of W type. Such large deviations of B type $LE_{\pi\pi^*}$ excitations are also observed previously by Wong and coworkers.[13,48] Kronik and coworkers[28] assigned those B type transitions as "charge-transfer-like" cases in which the occupied and unoccupied orbitals can be well separated by unitary transformation. The errors of W and B π–π^* valance excitations can be reduced by two optimally-tuned RSE functionals. To confirm the reliability of RI-CC2 as the benchmark method, we then compare the RI-CC2 excitation energies with those of EOM-CCSD(T) from the work of Szalay et al.[19] It can be seen that the RI-CC2 results are in good agreement with the EOM-CCSD(T) data, with MADs smaller than 0.1 eV for all three types of excitations. The double excitation contributions were found to be small through checking the diagnostic parameters for double excitations in RI-CC2 calculations (listed in Supporting Information), indicating that it is reasonable to calculate the excitation energies using tuned range-separated TDDFT. In addition, the sign "+" and "−" in Table 2 indicates that the calculated excitation energies are overestimated and underestimated, respectively, with respect to the reference values. By taking into account the sign of errors, the deviations of CT excitations from the two tuned RSE functionals (LC-ωPBE* and ωB97X*) can be further reduced with respect to the EOM-CCSD(T) data.

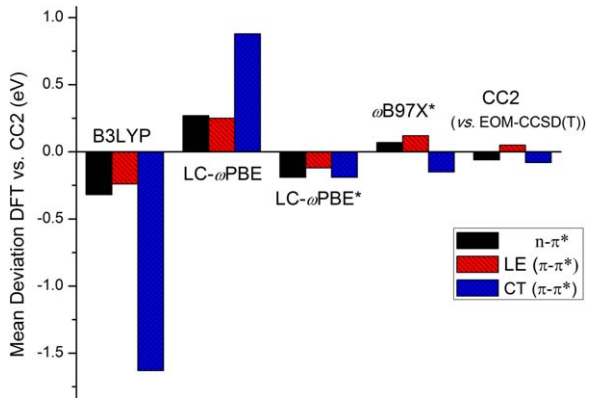

Figure 2. Histogram of mean deviations of various density functionals compared to those of RI-CC2 method. RI-CC2 values are compared to more accurate EOM-CCSD(T) data. Negative (positive) values indicate an underestimation (overestimation) of excitation energies with respect to the benchmarks.

Due to the efficiency of tuning using the golden ratio method in this work, we take the chance to perform the 2D tuning based on LC-ωPBE functional ($\alpha = 0.00$, $\omega = 0.400$ $Bohr^{-1}$) for GC_{WC} and GC_{ST}. Each optimal ω value was determined based on different α values from 0.00 to 0.60 as shown in Supporting Information Table S1. As α values increase the corresponding optimal ω values decrease. This can be attributed to the fact that at small r_{12} distance those functionals with large α values already include high percentages of eX and smaller ω values are needed to compensate for the relatively higher percentage of eX in the short-range region. As shown in Supporting Information Figure S3, the minimization of J^2 can be found as close to zero in the range of α from 0.00 to 0.50. When α exceeds 0.5, significantly large J^2 values exist even the tuning approach is performed. The result indicates that high percentage of eX (more than 50%) is not favorable to minimize J^2 and then to improve the quality of tuning. Interestingly, if zoom in the range of α from 0.00 to 0.50, we find that the J^2 values can be further reduced until practically zero which corresponds to the "optimal" α value. Through this way, the optimal α (and ω) is determined as 0.20 (0.194 $Bohr^{-1}$) for GC_{WC} and 0.16 (0.204 $Bohr^{-1}$) for GC_{ST}, respectively. Then we used the optimal 2D tuned functionals (LC-ωPBE-α*) to calculate the excitation energies (listed in Supporting Information Table S2). The LC-ωPBE-α* functional can produce slightly better description of excitation energies,

Table 3. Vertical excitation energies E_{ex} (eV) and oscillator strengths f (au) for 10 lowest singlet excited states of $GGCC_{DNA}$ and $AATT_{DNA}$ using different methods.

		ωB97X*			RI-CC2		B3LYP		
States	Transitions[a]	Type	E_{ex}	f	E_{ex}	f	Type	E_{ex}	f
	G_1C_2 C_1G_2				$GGCC_{DNA}$				
S_1	$G_1\ \pi \rightarrow \pi^*\ C_1$	CT	4.44	0.00	4.51	0.00	CT	2.80	0.00
S_2	$G_2\ \pi \rightarrow \pi^*\ C_2$	CT	4.67	0.00	4.76	0.00	CT	2.96	0.00
S_3	$G_1\ \pi \rightarrow \pi^*\ C_1$; $G_2\ \pi \rightarrow \pi^*\ C_2$	CT	4.81	0.00	4.88	0.00	CT	3.02	0.00
S_4	$G_1\ \pi \rightarrow \pi^*\ C_1$; $G_2\ \pi \rightarrow \pi^*\ C_2$	CT	4.85	0.01	4.92	0.03	CT	3.13	0.00
S_5	$G_1\ \pi \rightarrow \pi^*\ G_1$; $G_1\ \pi \rightarrow \pi^*\ C_2$	LE/CT	4.92	0.02	5.01	0.01	CT	4.19	0.00
S_6	$G_2\ \pi \rightarrow \pi^*\ G_2$; $C_2\ \pi \rightarrow \pi^*\ C_2$	LE	5.07	0.03	5.03	0.08	CT	4.26	0.00
S_7	$C_1\ \pi \rightarrow \pi^*\ C_1$; $C_2\ \pi \rightarrow \pi^*\ C_2$	LE	5.08	0.03	5.03	0.00	CT	4.30	0.00
S_8	$C_2\ \pi \rightarrow \pi^*\ C_2$; $C_1\ \pi \rightarrow \pi^*\ C_1$	LE	5.09	0.08	5.14	0.04	CT	4.34	0.00
S_9	$G_2\ \pi \rightarrow \pi^*\ G_2$	LE	5.28	0.13	5.40	0.00	CT	4.36	0.00
S_{10}	$C_1\ n \rightarrow \pi^*\ C_1$; $G_1\ n \rightarrow \pi^*\ C_1$	$n\pi^*$/CT	5.35	0.00	5.41	0.11	CT	4.39	0.00
	A_1T_2 T_1A_2				$AATT_{DNA}$				
S_1	$A_1\ \pi \rightarrow \pi^*\ A_1$; $A_2\ \pi \rightarrow \pi^*\ A_2$	LE	4.96	0.02	4.95	0.00	CT	3.94	0.00
S_2	$T_1\ n \rightarrow \pi^*\ T_1$	$n\pi^*$	5.00	0.00	5.01	0.00	CT	4.07	0.00
S_3	$T_2\ n \rightarrow \pi^*\ T_2$; $T_1\ \pi \rightarrow \pi^*\ T_1$	$n\pi^*$/LE	5.06	0.01	5.07	0.02	CT	4.24	0.00
S_4	$T_2\ n \rightarrow \pi^*\ T_2$	$n\pi^*$	5.07	0.00	5.17	0.01	CT	4.38	0.00
S_5	$T_1\ \pi \rightarrow \pi^*\ T_1$; $T_2\ \pi \rightarrow \pi^*\ T_2$	LE	5.10	0.20	5.23	0.04	LE	4.52	0.01
S_6	$A_1\ \pi \rightarrow \pi^*\ A_1$; $A_2\ \pi \rightarrow \pi^*\ A_2$	LE	5.16	0.02	5.26	0.00	LE/CT	4.65	0.02
S_7	$A_1\ \pi \rightarrow \pi^*\ A_1$; $A_2\ \pi \rightarrow \pi^*\ A_2$	LE	5.29	0.18	5.30	0.28	LE	4.65	0.00
S_8	$A_1\ \pi \rightarrow \pi^*\ A_1$; $A_2\ \pi \rightarrow \pi^*\ A_2$	LE	5.31	0.19	5.39	0.30	$n\pi^*$	4.73	0.01
S_9	$A_1\ n \rightarrow \pi^*\ A_1$	$n\pi^*$	5.36	0.03	5.44	0.03	$n\pi^*$	4.79	0.00
S_{10}	$A_2\ n \rightarrow \pi^*\ A_2$	$n\pi^*$	5.46	0.00	5.56	0.00	LE/CT	4.81	0.02

[a] Those transitions are assigned based on the results using optimally tuned ωB97X* functionals and the hole/electron distributions for each transition are presented in Supporting Information Figure S5.

particularly for n–π^* transitions, with respect to the corresponding 1D tuned LC-ωPBE* ($\alpha = 0.00$) due to the inclusion of eX in the short-range limit. The finding is consistent with recent studies by Raeber and Wong,[48] and Kronik and coworkers.[59] In this regard, the slightly better performance for ωB97X* in this work can also be attributed to its 16% short-range eX. However, considering the comparable accuracy of 1D tuning and the relatively expensive cost of 2D tuning, only 1D tuning based on the ωB97X functionals is employed through the following studies.

For the GC_{WC} base pair, both the RI-CC2 and EOM-CCSD(T) calculations show that the lowest allowed transition is localized on the guanine base, as seen in Table 2. The "bright" π–π^* transition with large oscillator strengths, can be assigned as a local excitation (LE) located at guanine. The CT transition is found with the HOMO located on guanine and the LUMO on cytosine. For the stacked GC_{ST} molecule, the ordering of the lowest excited states changes compared to the GC_{WC} and the lowest transition can be assigned as the π–π^* transition on cytosine. It should be noted that B3LYP functional incorrectly predicts the lowest excited state of GC_{ST} and GC_{WC} as CT excitations while all the RSE functionals correctly recognize the LE character of the lowest excited states. For AT_{WC} and AT_{ST}, the lowest excited states are assigned as the n–π^* transitions located on thymine bases. The B3LYP functional still fails to describe the character of lowest excited state and incorrectly predict it as a CT transition. The n–π^* excitation energies in AT_{WC} pair are smaller than those in the stacked pair. This can be explained by the fact that the lone pairs on the oxygen atoms play a more important role in the formation of hydrogen bonds than the stacking interactions.[19] The CT excitation energies of AT_{ST} are significantly smaller than those of AT_{WC} but the corresponding oscillator strengths is somewhat larger. This is mainly due to the influence by the π–π^* stacking interactions resulting a more ionic character between adenine and thymine.

In a realistic DNA model, both the WC H-bonding and π-stacking interactions exist and can act simultaneously. The models of WC or ST dimers are apparently not enough and the tetramer model including the two types of interactions can be approximately considered as the basic building blocks of a DNA duplex. We then calculate the excitation energies and the corresponding oscillator strengths of four tetramers using optimally-tuned ωB97X* functionals. Results of $AATT_{DNA}$ and $GGCC_{DNA}$ are shown in Table 3 and those of $ATTA_{DNA}$ and $GCCG_{DNA}$ are presented in Supporting Information Table S3. Results using B3LYP functional are also calculated for the sake of comparison. Calculations based on more reliable but expensive RI-CC2 method are performed for $AATT_{DNA}$ and $GGCC_{DNA}$ and only 10 lowest excited states are computed. The absorption spectra were also simulated as illustrated in Figure 3 and Supporting Information Figure S4. First, as seen in Figure 3, both the excitation energies and oscillator strengths calculated by ωB97X* agree reasonably well with the results of RI-CC2 for 10 lowest singlet excited states. However, B3LYP functional completely fails to predict the excited states of larger tetramers. The 10 lowest excitation energies calculated by B3LYP are obviously below the RI-CC2 data as large as > 1.0 eV and their resulting oscillator strengths of 10 lowest excited states are almost zero. For $GGCC_{DNA}$, the B3LYP functional arbitrarily predict all the 10 lowest excited states as

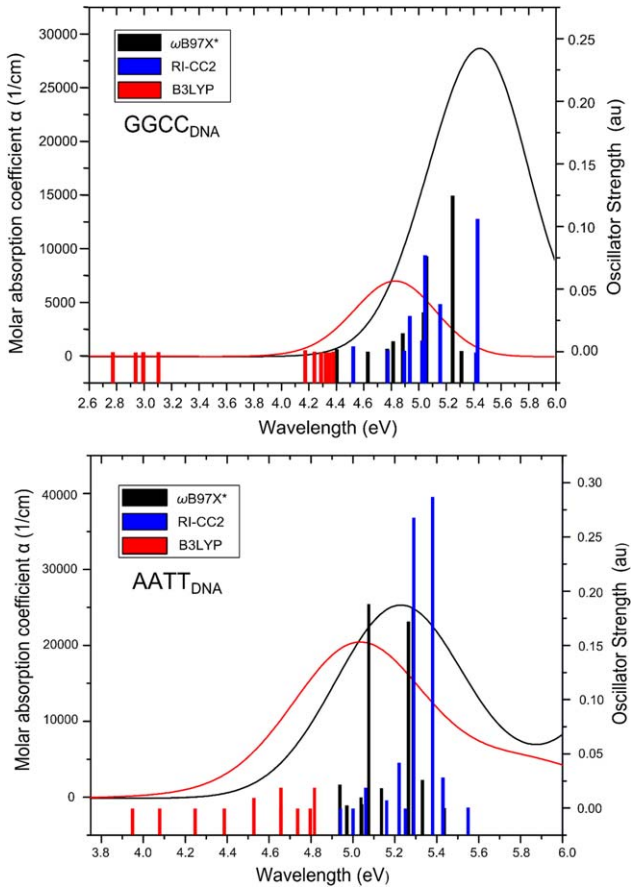

Figure 3. Simulated electronic absorption spectra of $GGCC_{DNA}$ and $AATT_{DNA}$, the corresponding oscillator strengths of 10 lowest singlet excited states are also included: red columns for B3LYP; blue columns for RI-CC2; and black columns for ωB97X*. [Color figure can be viewed in the online issue, which is available at wileyonlinelibrary.com.]

CT excitations. The strongest transition using ωB97X* functional is found at the 12th singlet excited state with the excitation energy of 5.43 eV ($f = 0.25$) and can be assigned as the mixture of LE ($G_1\ \pi \rightarrow \pi^*\ G_1$) and CT ($G_1\ \pi \rightarrow \pi^*\ G_2$) transitions. A very close excitation energy of 5.43 eV at the maximum absorption ($f = 0.44$) is found for $GCCG_{DNA}$ and this strong transition can be assigned as localized excitation ($G_2\ \pi \rightarrow \pi^*\ G_2$) on guanine. The excitation energies at maximum absorption for $GGCC_{DNA}$ and $GCCG_{DNA}$ calculated by B3LYP are significantly underestimated by roughly 0.4∼0.6 eV compared to those of ωB97X* functional. For AT tetramers, similar failures using B3LYP are observed, however, the differences between the results of ωB97X* and B3LYP are not obvious. As shown in Figure 3 and Supporting Information Figure S4, the absorption peaks for $AATT_{DNA}$ and $ATTA_{DNA}$ by B3LYP are only 0.2∼0.3 eV red-shifted compared to those of ωB97X* functional and the calculated oscillator strengths are also improved. Interestingly, the CT transition is not observed in the 10 lowest singlet excited states of $AATT_{DNA}$ based on the results of ωB97X*, however, the B3LYP functional predicts the 4 lowest excited states as CT excitations. Furthermore, one can observe more CT characters in the 10 lowest excited states of GC tetramers while there are more localized excitations (such as $\pi\pi^*$ and $n\pi^*$) in AT tetramers. This finding can explain why B3LYP functional perform reasonably better description of absorption spectra of AT tetramers than those of GC tetramers. Overall, significant improvements in predicting excitation energies and oscillator strengths of both AT/GC dimers and larger tetramers are found by using the optimally-tuned ωB97X* functional. In addition, it is also important to mention that the very high costs of RI-CC2 and EOM-CCSD(T) calculations currently preventing their applications on a larger DNA system in this work. The optimally tuning approach therefore shows a clear advantage because of reasonable computational cost.

Next, we explain why various density functionals have quite different performance on the calculations of excitation energies. First, as seen in Figure 4a, the percentages of exact-exchange as a function of interelectronic distance were plotted for various functionals used in this work. At r_{12} around 3 atomic units (∼ 1.58 Å) which approaches carbon-carbon single bond length, both the two tuned functionals (LC-ωPBE* and ωB97X*) afford roughly 65% eX. The non-tuned LC-ωPBE and ωB97X give higher percentages of 90% and 80% eX, respectively, indicating they are more "HF-like" method.[60] The pure HF method with 100% eX is known to be a strong localization of electronic structure due to ignoring the role of electron correlation. The B3LYP functional includes only 20% eX, which is still too low and makes it somewhat delocalized. It can be seen that both high and low percentages of eX included in the functionals will result significant errors. Second, it is well-known that issues with DFT are closely connected to violations of basic conditions of constraints in the exact KS theory.[61] For instance, conventional density functionals always overestimate/underestimate the effect of delocalization of holes/electrons. In exact KS theory, the energy of an atom or molecule as a function of electron number *E(N)* should afford straight-line segments between integers.[62] Therefore, the curvature of *E(N)* is indicative of the so-called delocalization error (DE).[61] Here, as shown in Figure 4b, we examine the behavior of *E(N)* for GC_{WC} as a representative example. The results are closely related to the finding of eX percentages in Figure 4a.

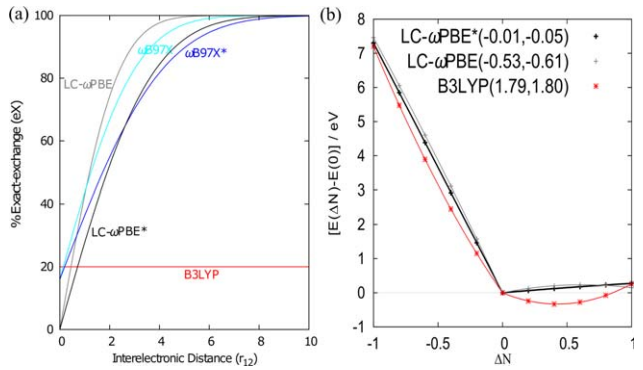

Figure 4. a) Percentages of exact-exchange (eX) as a function of interelectronic distance (r_{12}), the curves of LC-ωPBE* and ωB97X*are plotted for GC_{WC} with the ω values of 0.251 and 0.218, respectively; b) Energy of GC_{WC} as a function of fractional electron number, ΔN, relative to neutral system ($\Delta N = 0$). The numerical values in the plot correspond to the coefficients of $(\Delta N)^2$ of quadratic fits to *E(N)* in the electron-deficient and electron-rich regime, respectively ($\Delta N < 0$, $\Delta N > 0$). [Color figure can be viewed in the online issue, which is available at wileyonlinelibrary.com.]

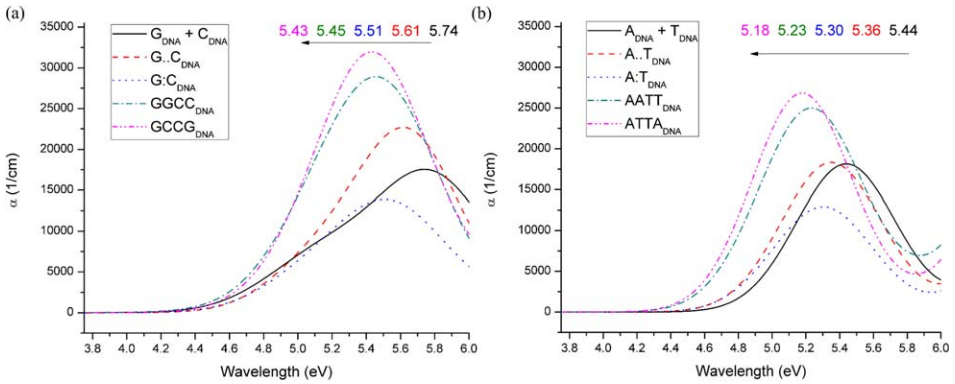

Figure 5. Simulated absorption spectra of various DNA pairs and tetramers extracted from the X-ray structures using the optimally tuned ωB97X* functional and cc-pVTZ basis set. [Color figure can be viewed in the online issue, which is available at wileyonlinelibrary.com.]

Global hybrid B3LYP produce large positive curvature of *E(N)*, indicating that it is too delocalized. For LC-ωPBE functional, the behavior of DE is more improved but it still affords an obvious negative curvature, showing a localized character. Overall, the optimally tuned LC-ωPBE* can greatly eliminate DEs and the tuning procedure appears to be successful in terms of vanishing DE values. Here, we emphasize again that an "ideal" amount of eX included in density functionals is necessary to obtain accurate results.

Due to the efficiency and accuracy of tuning method, the effects induced by the H-bonding and π-stacking interactions in DNA dimers and tetramers are quantitatively investigated using the ωB97X* functional by simulating the absorption spectra. Krylov and coworkers[52] demonstrated that there is a cooperative effect between H-bonding and stacking interactions through studying ionization potentials of $AATT_{DNA}$ tetramer and further assigned it as the crossing (electrostatic) interactions between the diagonal bases. In this work, the simulated absorption spectra are presented in the range from 3.8 to 6.0 eV where most intense peaks in low-energy region appear. The calculated peak positions of WC pairs with H-bonding interactions ($A.T_{DNA}$, $G.C_{DNA}$) and the stacked complexes with π-stacking interactions ($A{:}T_{DNA}$, $G{:}C_{DNA}$) are also listed in Figure 5, as well as the linear combination of the photoabsorption cross sections from the isolated bases ($A_{DNA}+T_{DNA}$, $G_{DNA}+C_{DNA}$). Therefore, the effects induced by the H-bonding and π-stacking interactions can be revealed according to the shifts of the intense peaks. In GC dimers, the stacking effect ($\Delta = 0.23$ eV) is more pronounced than the H-bonding interaction ($\Delta = 0.13$ eV) with respect to the peak of $G_{DNA}+C_{DNA}$. Similarly in AT dimers, the effect of stacking in A:T ($\Delta = 0.14$ eV) is also stronger than that of H-bonding in A.T ($\Delta = 0.08$ eV). This is mainly due to the formation of a more delocalized electronic structure in the stacked configuration. Furthermore, we studied the peaks shifts of larger tetramers where H-bonding and stacking effects are active simultaneously as shown in Figure 6. In $ATTA_{DNA}$, firstly assuming there are no interactions between the four isolated bases, the H-bonding results a red-shift of -0.08 eV and the stacking causes a decrease in the peak position of 0.14 eV. The additivity of the two effects is -0.22 eV compared to the shift of -0.26 eV in $ATTA_{DNA}$. Thus, the -0.04 eV can be attributed to the cooperative effect of H-bonding and stacking interactions. For $AATT_{DNA}$, the H-bonding of $A.T_{DNA}$ still results a red-shift of -0.08 eV and the stacking effect from the homodimers ($A{:}A_{DNA}$ and $T{:}T_{DNA}$) causes a decrease of 0.12 eV (Supporting Information Table S4). The sum of two effects is -0.20 eV compared to the shift of -0.21 eV in $AATT_{DNA}$. Therefore, the computed cooperativity in $AATT_{DNA}$ is -0.01 eV which is less pronounced than that in $ATTA_{DNA}$. This result is consistent with the finding by Krylov et al.[52] Through the same way, we also studied the cooperativity for GC tetramers and the computed values are $+0.15$ eV for $GGCC_{DNA}$ and $+0.05$ eV for $GCCG_{DNA}$. However, unlike the cooperative effects in AT tetramers contributing in the further red-shift of peaks, the cooperativity in GC tetramers conversely makes the corresponding peaks blue shift. We speculate the difference in cooperativity of GC and AT tetramers is due to the excessively stronger interactions of H-bonding and stacking in GC tetramers. The stronger interactions in GC tetramers than those in AT tetramers can be intuitively reflected from the maps of electrostatic potential surfaces (ESP) as shown in Supporting Information Figure S6. ESP maps are very useful to visualize the charge distributions and electrostatic interactions in three dimensional diagrams of complex molecules. The red color as the lowest electrostatic potential energy value and the blue as the highest one are employed to interpret the varying intensities of the electrostatic potential energy values.

In experiment, the UV absorption of DNA duplex is increased when the two single DNA strands are being separated upon denaturation and then many bases are in free form and do not form hydrogen bonds with complementary bases. This phenomenon is known as the hyperchromicity effect and the inverse process is called hypochromicity effect. A recent combined theoretical-experimental study by D'Abramo et al.[63] also captures the phenomenon of hypochromicity on the denaturation of a polyA–polyT double strand. Here, with the assistance of optimally-tuned RSE functional, we also get the chance to (semi-)quantitatively study the hypochromicity effect by analysis of absorption intensity (molar absorption coefficient) of various DNA tetramers. The molar absorption coefficients for all the systems are calculated and listed in Supporting Information Table S4. As shown in Figure 5, compared to the sum of peak intensities of isolated bases, the H-bonding interactions ($A.T_{DNA}$ and

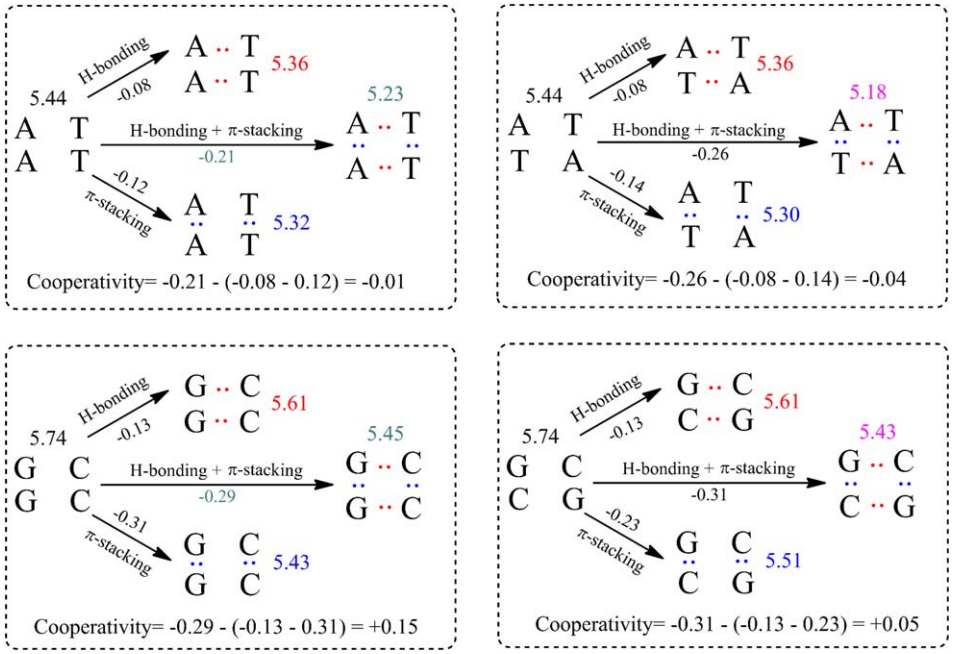

Figure 6. Schematic diagram of cooperative effect in various DNA tetramers and all the values (in eV) in the figure correspond to the excitation energies of intense peaks calculated by ωB97X* functional. [Color figure can be viewed in the online issue, which is available at wileyonlinelibrary.com.]

G.C_{DNA}) result an enhancement of the absorption intensity but the stacking interactions (A:T_{DNA} and G:C_{DNA}) conversely reduce the intensity. Interestingly, for various tetramers in which the H-bonding and π-stacking interactions are combined, the absorption intensities of linear combinations of four isolated bases ($A_{DNA} + T_{DNA} + A_{DNA} + T_{DNA}$ and $G_{DNA} + C_{DNA} + G_{DNA} + C_{DNA}$) are consistently larger than those of various tetramers ($AATT_{DNA}$, $ATTA_{DNA}$, $GGCC_{DNA}$, and $GCCG_{DNA}$). This finding is in agreement with the experimental evidence where four isolated bases correspond to the free-form bases after denatured and the various tetramers randomly extracted from X-ray structure of water-solvated DNA duplex are approximately considered as the basic building block of DNA helix. The decrease of absorption intensity (hypochromicity effect) can be explained by the fact that the effect of stacking interaction is stronger than that of H-bonding. This result agrees with the finding of Danilov and Volkov.[64] In addition, this work presents another example of the existence of cooperative effect between H-bonding and stacking interactions by studying the shifts of absorption peaks, the changes of molar absorption coefficients and the resulting hypochromicity effect.

Conclusions

In this work, we have demonstrated the reliability and efficiency of optimally-tuned RSE functional in the prediction of excited states of various DNA dimers and tetramers. Especially the excitation energies of three types of transitions ($n\pi^*$, $LE_{\pi\pi^*}$, and $CT_{\pi\pi^*}$), as well as the corresponding oscillator strengths, can be well predicted and the results are comparable with respect to high-level RI-CC2 and EOM-CCST(T) benchmarks. The RSE functionals with optimally tuned (usually smaller) ω values significantly outperform their default version. Furthermore, the larger mean absolute derivations by the widely-used B3LYP functional can be attributed to the lack of long-range exchange interactions and large delocalization error. The large errors of non-tuned RSE functional are mainly due to their high percentages of exact exchange. The impacts of H-bonding and π-stacking interactions are analyzed by the simulated UV absorption spectra of both relaxed and unrelaxed DNA dimers and tetramers using the optimally-tuned ωB97X* functional. The hypochromicity effect is investigated in the models of DNA base tetramers and the result shows that the stacking interaction, instead of H-bonding interaction, makes the main contribution to the hypochromicity. Overall, the present work has demonstrated a reliable theoretical tool for characterization of excited states of DNA base dimers and tetramers. It is potentially interesting to explore this tuning method in a longer DNA helix or large biological system due to its efficiency and accuracy. Furthermore, a reliable first-principle evaluation of the effective electronic couplings (hole/electron mobility) in DNA-based nanoelectronics is urgently required and we reserve those issues for subsequent studies.

Keywords: DFT/TDDFT · range-separated · optimal tuning

How to cite this article: H. Sun, S. Zhang, C. Zhong, Z. Sun *J. Comput. Chem.* **2016**, *37*, 684–693. DOI: 10.1002/jcc.24266

Additional Supporting Information may be found in the online version of this article.

[1] J. D. Watson, F. H. C. Crick, *Nature* **1953**, *171*, 737.
[2] C. E. Crespo-Hernandez, B. Cohen, B. Kohler, *Nature* **2005**, *436*, 1141.
[3] G. C. Schatz, *J. Phys. Chem. Lett.* **2010**, *1*, 2054.

[4] B. N. G. Giepmans, S. R. Adams, M. H. Ellisman, R. Y. Tsien, *Science* **2006**, *312*, 217.
[5] S. Mallajosyula, S. Pati, *J. Phys. Chem. Lett.* **2010**, *1*, 1881.
[6] G. C. Schatz, *J. Phys. Chem. Lett.* **2012**, *3*, 3663.
[7] C. Ko, S. Hammes-Schiffer, *J. Phys. Chem. Lett.* **2013**, *4*, 2540.
[8] T. Gustavsson, R. Improta, D. Markovitsi, *J. Phys. Chem. Lett.* **2010**, *1*, 2025.
[9] J. C. Genereux, J. K. Barton, *Nat. Chem.* **2009**, *1*, 106.
[10] O. S. Lee, T. R. Prytkova, G. C. Schatz, *J. Phys. Chem. Lett.* **2010**, *1*, 1781.
[11] Y. A. Berlin, A. A. Voityuk, M. A. Ratner, *ACS Nano* **2012**, *6*, 8216.
[12] L. Jensen, N. Govind, *J. Phys. Chem. A* **2009**, *113*, 9761.
[13] M. E. Foster, B. M. Wong, *J. Chem. Theory Comput.* **2012**, *8*, 2682.
[14] J. B. Schimelman, D. M. Dryden, L. Poudel, K. E. Krawiec, Y. Ma, R. Podgornik, V. A. Parsegian, L. K. Denoyer, W. Y. Ching, N. F. Steinmetz, R. H. French, *Phys. Chem. Chem. Phys.* **2015**, *17*, 4589.
[15] D. Varsano, R. Di Felice, M. A. L. Marques, A. Rubio, *J. Phys. Chem. B* **2006**, *110*, 7129.
[16] B. Kohler, *J. Phys. Chem. Lett.* **2010**, *1*, 2047.
[17] F. A. Miannay, Á. Bányász, T. Gustavsson, D. Markovitsi, *J. Am. Chem. Soc.* **2007**, *129*, 14574.
[18] H. Sun, S. Zhang, Z. Sun, *Phys. Chem. Chem. Phys.* **2015**, *17*, 4337.
[19] P. G. Szalay, T. Watson, A. Perera, V. Lotrich, R. J. Bartlett, *J. Phys. Chem. A* **2013**, *117*, 3149.
[20] M. Barbatti, A. J. A. Aquino, J. J. Szymczak, D. Nachtigallova, P. Hobza, H. Lischka, *Proc. Natl. Acad. Sci. USA* **2010**, *107*, 21453.
[21] C. Crespo-Hernandez, B. Cohen, P. Hare, B. Kohler, *Chem. Rev.* **2004**, *104*, 1977.
[22] P. G. Szalay, T. Watson, A. Perera, V. F. Lotrich, R. J. Bartlett, *J. Phys. Chem. A* **2012**, *116*, 6702.
[23] A. A. Voityuk, *J. Chem. Theory Comput.* **2014**, *10*, 4950.
[24] D. Kánnár, P. G. Szalay, *J. Chem. Theory Comput.* **2014**, *10*, 3757.
[25] M. A. L. Marques, C. A. Ullrich, F. Nogueira, A. Rubio, K. Burke, E. K. U. Gross, Time-Dependent Density Functional Theory, Vol. *706*; Springer: Berlin, Germany, **2006**.
[26] E. Runge, E. K. U. Gross, *Phys. Rev. Lett.* **1984**, *52*, 997.
[27] J. Autschbach, *ChemPhysChem* **2009**, *10*, 1757.
[28] N. Kuritz, T. Stein, R. Baer, L. Kronik, *J. Chem. Theory Comput.* **2011**, *7*, 2408.
[29] T. Shimazaki, Y. Asai, *Chem. Phys. Lett.* **2008**, *466*, 91.
[30] A. Dreuw, M. Head-Gordon, *J. Am. Chem. Soc.* **2004**, *126*, 4007.
[31] L. Goerigk, S. Grimme, *J. Chem. Theory Comput.* **2011**, *7*, 3272.
[32] J. Autschbach, M. Srebro, *Acc. Chem. Res.* **2014**, *47*, 2592.
[33] D. J. Tozer, *J. Chem. Phys.* **2003**, *119*, 12697.
[34] T. Yanai, D. P. Tew, N. C. Handy, *Chem. Phys. Lett.* **2004**, *393*, 51.
[35] H. Iikura, T. Tsuneda, T. Yanai, K. Hirao, *J. Chem. Phys.* **2001**, *115*, 3540.
[36] A. Savin, In Recent Developments and Applications of Modern Density Functional Theory, Vol. *4*; J. M. Seminario, Ed.; Elsevier: Amsterdam, **1996**; pp. 327–357.
[37] Y. Tawada, T. Tsuneda, S. Yanagisawa, T. Yanai, K. Hirao, *J. Chem. Phys.* **2004**, *120*, 8425.
[38] A. W. Lange, M. A. Rohrdanz, J. M. Herbert, *J. Phys. Chem. B* **2008**, *112*, 6304.
[39] H. Sun, J. Autschbach, *ChemPhysChem* **2013**, *14*, 2450.
[40] U. Salzner, A. Aydin, *J. Chem. Theory Comput.* **2011**, *7*, 2568.
[41] L. Kronik, T. Stein, S. Refaely-Abramson, R. Baer, *J. Chem. Theory Comput.* **2012**, *8*, 1515.
[42] R. Baer, D. Neuhauser, *Phys. Rev. Lett.* **2005**, *94*, 043002.
[43] T. Körzdörfer, J. S. Sears, C. Sutton, J. L. Brédas, *J. Chem. Phys.* **2011**, *135*, 204107.
[44] H. Sun, J. Autschbach, *J. Chem. Theory Comput.* **2014**, *10*, 1035.
[45] R. Baer, E. Livshits, U. Salzner, *Annu. Rev. Phys. Chem.* **2010**, *61*, 85.
[46] M. Levy, J. P. Perdew, V. Sahni, *Phys. Rev. A* **1984**, *30*, 2745.
[47] B. Moore, A. Charaf-Eddin, A. Planchat, C. Adamo, J. Autschbach, D. Jacquemin, *J. Chem. Theory Comput.* **2014**, *10*, 4599.
[48] A. E. Raeber, B. M. Wong, *J. Chem. Theory Comput.* **2015**, *11*, 2199.
[49] M. Srebro, J. Autschbach, *J Phys. Chem. Lett.* **2012**, *3*, 576.
[50] J. Šponer, P. Jurečka, P. Hobza, *J. Am. Chem. Soc.* **2004**, *126*, 10142.
[51] N. Narayana, M. A. Weiss, *J. Mol. Biol.* **2009**, *385*, 469.
[52] K. B. Bravaya, E. Epifanovsky, A. I. Krylov, *J. Phys. Chem. Lett.* **2012**, *3*, 2726.
[53] H. Karabyk, R. Sevincek, H. Karabyk, *Phys. Chem. Chem. Phys.* **2014**, *16*, 15527.
[54] R. Ahlrichs, M. Bär, M. Häser, H. Horn, C. Kölmel, *Chem. Phys. Lett.* **1989**, *162*, 165.
[55] M. Valiev, E. J. Bylaska, N. Govind, K. Kowalski, T. P. Straatsma, H. J. J. Van Dam, D. Wang, J. Nieplocha, E. Apra, T. L. Windus, W. A. de Jong, *Comput. Phys. Commun.* **2010**, *181*, 1477.
[56] O. A. Vydrov, G. E. Scuseria, *J. Chem. Phys.* **2006**, *125*, 234109.
[57] J. D. Chai, M. Head-Gordon, *J. Chem. Phys.* **2008**, *128*, 084106.
[58] M. J. Frisch, G. W. Trucks, H. B. Schlegel, G. E. Scuseria, M. A. Robb, J. R. Cheeseman, G. Scalmani, V. Barone, B. Mennucci, G. A. Petersson, H. Nakatsuji, M. Caricato, X. Li, H. P. Hratchian, A. F. Izmaylov, J. Bloino, G. Zheng, J. L. Sonnenberg, M. Hada, M. Ehara, K. Toyota, R. Fukuda, J. Hasegawa, M. Ishida, T. Nakajima, Y. Honda, O. Kitao, H. Nakai, T. Vreven, J. A. Montgomery, Jr., J. E. Peralta, F. Ogliaro, M. J. Bearpark, J. Heyd, E. N. Brothers, K. N. Kudin, V. N. Staroverov, R. Kobayashi, J. Normand, K. Raghavachari, A. P. Rendell, J. C. Burant, S. S. Iyengar, J. Tomasi, M. Cossi, N. Rega, N. J. Millam, M. Klene, J. E. Knox, J. B. Cross, V. Bakken, C. Adamo, J. Jaramillo, R. Gomperts, R. E. Stratmann, O. Yazyev, A. J. Austin, R. Cammi, C. Pomelli, J. W. Ochterski, R. L. Martin, K. Morokuma, V. G. Zakrzewski, G. A. Voth, P. Salvador, J. J. Dannenberg, S. Dapprich, A. D. Daniels, Ö. Farkas, J. B. Foresman, J. V. Ortiz, J. Cioslowski, D. J. Fox, Gaussian 09; Gaussian, Inc.: Wallingford, CT, **2009**.
[59] D. A. Egger, S. Weissman, S. Refaely-Abramson, S. Sharifzadeh, M. Dauth, R. Baer, S. Kümmel, J. B. Neaton, E. Zojer, L. Kronik, *J. Chem. Theory Comput.* **2014**, *10*, 1934.
[60] B. Kirtman, S. Bonness, A. Ramirez-Solis, B. Champagne, H. Matsumoto, H. Sekino, *J. Chem. Phys.* **2008**, *128*, 114108.
[61] A. J. Cohen, P. Mori-Sánchez, W. Yang, *Science* **2008**, *321*, 792.
[62] Y. Imamura, R. Kobayashi, H. Nakai, *J. Chem. Phys.* **2011**, *134*, 124113.
[63] M. D'Abramo, C. L. Castellazzi, M. Orozco, A. Amadei, *J. Phys. Chem. B* **2013**, *117*, 8697.
[64] V. I. Danilov, S. N. Volkov, *Biopolymers* **1975**, *14*, 1205.

Received: 8 September 2015
Revised: 10 November 2015
Accepted: 11 November 2015
Published online on 15 December 2015